Journal Pre-proof

Anisotropic rate-dependent mechanical behavior of Poly(Lactic Acid) processed by Material Extrusion Additive Manufacturing
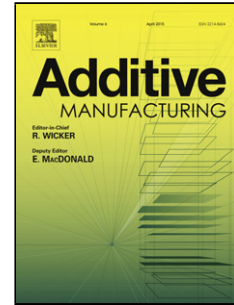
Wilco M.H. Verbeeten, Miriam Lorenzo-Bañuelos, Pablo J. Arribas-Subiñas

Please cite this article as: Wilco M.H. Verbeeten, Miriam Lorenzo-Ba\ {n}uelos, Pablo J. Arribas-Subi\ {n}as, , Anisotropic rate-dependent mechanical behavior of Poly(Lactic Acid) processed by Material Extrusion Additive Manufacturing, *<![CDATA[Additive Manufacturing]]>* (2019), doi: https://doi.org/10.1016/j.addma.2019.100968

Anisotropic rate-dependent mechanical behavior of Poly(Lactic Acid) processed by Material Extrusion Additive Manufacturing

Wilco M.H. Verbeeten[a,*], Miriam Lorenzo-Bañuelos[a], Pablo J. Arribas-Subiñas[b]

[a]*Structural Integrity Research Group, Universidad de Burgos, Avenida Cantabria s/n, E-09006, Burgos, Spain*
[b]*Escuela Politécnica Superior, Universidad de Burgos, Avenida Cantabria s/n, E-09006, Burgos, Spain*

Abstract

The strain-rate dependence of the yield stress for Material Extrusion Additive Manufacturing (ME-AM) polylactide samples was investigated. Apparent densities of the ME-AM processed tensile test specimens were measured and taken into account in order to study the effects of the ME-AM processing step on the material behavior. Three different printing parameters were changed to investigate their influence on mechanical properties, *i.e.* infill velocity, infill orientation angle, and bed temperature. Additionally, compression molded test samples were manufactured in order to determine bulk properties, which have been compared to the ME-AM sample sets. Anisotropy was detected in the strain-rate dependence of the yield stresses. ME-AM samples with an infill angle of $0°$ have a higher strain-rate dependence than specimens with $\alpha_{or} = 90°$. Remarkably, the strain-rate dependence manifested by the ME-AM samples is considerably lower than that displayed by compression molded test specimens. The Ree-Eyring modification of the Eyring flow rule is able to accurately describe the strain-rate dependence of the yield stresses, taking two molecular deformation processes into account to describe the yield kinetics. The results from this paper further show a change from a brittle behavior in case of compression molded samples to a semi-ductile behavior for some of the ME-AM sample sets. This change is attributed to the processing phase and stresses the importance that the temperature profile (initial fast cooling combined with successive heating cycles) and the strain profile during ME-AM processing have on the resulting mechanical properties. Both these profiles are significantly different from the thermo-mechanical history that material elements experience during conventional processing methods, *e.g.* injection or compression molding. This paper can be seen as initial work that can help to further develop predictive numerical tools for Material Extrusion Additive Manufacturing, as well as for the design of structural components.

Keywords: PLA, print velocity, infill orientation, bed temperature, anisotropic strain-rate dependent yield stress, Eyring rate equation

---

*Corresponding author
Email address: wverbeeten@ubu.es (Wilco M.H. Verbeeten)

1. Introduction

Additive Manufacturing (AM) is a relatively new and rapidly upcoming production process, which has gained increasing interest from both industry as well as academic communities. Over the last couple of decades, development and improvement of the technologies have led to a modest shift from Rapid Prototyping (RP) for the production of presentation models, and still the main AM application, towards Rapid Manufacturing (RM) for the fabrication of end-use parts [1]. For polymer materials, Material Extrusion Additive Manufacturing (ME-AM) [2] is one of the most popular techniques, as it facilitates the fabrication of customized end-use products at low investment costs [3, 4]. ME-AM is the term used in the ISO and ASTM standard [2] and includes, among others, similar technologies indicated by terms such as Fused Deposition Modeling (FDM ®), Fused Filament Fabrication (FFF), Fused Layer Modeling (FLM), or 3D printing.

Several reviews are availabe for engineers and researchers to introduce themselves into Additive Manufacturing, *e.g.* Ngo *et al.* [5]. A review focused more specifically on polymer materials was written by Wendel *et al.* [6]. And a more recent review on polymers was written by Dizon *et al.* [4]. Turner *et al.* [3] wrote a review of ME-AM, while Mackay [7] concentrated on the rheological behavior. An even more specific review was elaborated by Liu *et al.* [8] focussing on PLA. Wendel *et al.* [6] expected that in the near future, the optimization of process parameters would lead to ME-AM parts with similar mechanical properties as injection or compression molded parts. Several research groups, *e.g.* Spoerk *et al.* [9] and Song *et al.* [10], have shown that this is already a reality.

Material Extrusion Additive Manufacturing is a technology where a thermoplastic polymer filament is pushed through a heated liquefier by a pinch roller mechanism. The molten polymer is extruded through a heated nozzle, and deposited onto a (heated) build platform or an already deposited layer, where it quickly solidifies [3, 11]. By controlling the position of the heated nozzle and bed, complex 3D objects can be produced. The final result is a laminate composite structure with stacked layers consisting of partially bonded filaments with interstitial voids [12, 13]. In the remainder of the text, the term strand will be used to refer to an extruded and deposited filament.

For load-bearing applications of polymers, components need a minimum of mechanical properties. Ideally, one would like to be able to quantitatively predict these mechanical properties from the component's shape and printer parameter settings as given in the slicer program. That is, however, a tremendous and enormously complex task. One has to consider, that the final macroscopic behavior of ME-AM parts is, similar to parts fabricated with more conventional polymer processing methods (*e.g.* injection molding, compression molding, melt extrusion, blow molding), governed by the onset of plastic strain localization [14, 15, 16]. In turn, this is dominated by the *local* large strain intrinsic properties, known to be inhomogeneous along a product's geometry [17, 18, 19]. This heterogeneity is a result of the different thermo-mechanical history, *i.e.* changing temperatures, pressures and strains as a function of time, a material element experiences at distinct locations in the component. Hence, the final prop-

2

erties of ME-AM parts are bound by the same polymer physics as any other polymer
45   processing method [20].

However, due to the particularity of the ME-AM process, the resulting final part
is generally voided and has both bulk-like (within a strand) as well as non-bulk-like
(in strand-to-strand bonds) properties [20]. ME-AM parts can demonstrate significant
differences in stiffness and strength in the direction of a strand and perpendicular to
50   the strand direction [12]. Consequently, structural integrity of ME-AM parts is mostly
determined by that latter weaker direction, *i.e.* the bond strength between adjacent and
stacked strands [11]. Therefore, in order to predict macroscopic mechanical properties
in a quantitative way, four aspects should be considered both spatially as well as tem-
porally: (i) the mesostructure, (ii) temperature, (iii) strain, and (iv) pressure. Besides,
55   these are all greatly influenced by the chosen printing parameters.

As was shown by Rodriguez *et al.* [21, 12], and more recently by Abbott *et al.*
[11], the resulting mesostructure of ME-AM parts is a key controlling parameter to
influence mechanical properties. A strand will spread into an oblong shape, which
final shape depends on the printing parameters and the relative surface energies of the
60   strand and the surface on which it is printed [3]. Consecutively, the oblong shape of the
strand determines the contact area and the resultant bond length. The effect of printing
parameters, such as extruder temperature, print speed, layer height, orientation [11],
as well as fiber width, strand-to-strand gap (distance between adjacent strands or air
gap), and interlayer configuration (skewed/aligned) [21] was investigated and related
65   to final bond length and mechanical properties. Higher bond lengths will generally lead
to improved strength [12, 11], while temperature tends to help to improve strength with
an equal relative bond length [11].

The temperature profile a material element experiences in a ME-AM part is an-
other key aspect to influence structural integrity. The thermal history in ME-AM
70   parts is highly non-isothermal due to the initial fast cooling, with cooling rates up to
$100\ ^oC\ s^{-1}$ [22], and successive heating during the consecutive deposition of strands.
This leads to temperature fluctuations near or around the glass transition temperature
T_g [23, 13, 20, 22, 24, 25, 11]. Since temperature determines molecular chain mobil-
ity, it directly influences rheological behavior, *i.e.* viscosity, reptation, crystallization
75   (if possible) and thermodynamic state. Hence, it regulates the final strand's oblong
shape and determines the weld strength, or bond strength, between strands, as that is
governed by the wetting and molecular diffusion at the interface driven by reptation
[26, 7, 25]. Furthermore, the thermo-mechanical history affects the crystallization pro-
cess [27, 28, 29, 30], thus influencing mechanical properties [31, 32, 33, 34, 35, 25,
80   36, 37]. Finally, Abbott *et al.* [11] indicated that the specimen geometry is expected
to also have an impact on temperature as a function of time, as the time between suc-
cesive strand depositions will influence the amount of time above the glass transition
temperature T_g [3], temperature above which molecular chain mobility is significantly
enhanced.

85   During the ME-AM process, shear effects in the nozzle and due to the curvature
between the nozzle and the strand will lead to orientation and stretch of the polymer
chain [38, 35, 7] in a non-uniform way along a strand's cross-section. Shear rates are of
order $100\ s^{-1}$ [22, 37] and can vary from under $100\ s^{-1}$ to upto $1000\ s^{-1}$, depending
on printing speeds [39]. Peng *et al.* [24] visualized the flow profile by inserting pigment

3

into a filament and they also concluded that the extrusion speed affects the velocity profile of the filament leaving the nozzle. In order to take orientation and stretch of the polymer chain molecule during processing into account, one needs to use adequate (molecularly-aware) constitutive models [38, 35] in a transient sense, such as *e.g.* the Giesekus [40], Phan-Thien-Tanner [41, 42], extended Pom-Pom [43, 44], Molecular Stress Function [45], or Rolie-Poly [46] models. It was shown by Rodriguez *et al.* [12] that differences in molecular orientation produce different mechanical properties in ME-AM components.

Together with shear effect, the heated liquefier and nozzle zone is also the location of pressure build up as the solid filament acts as a piston and pushes the molten material through the nozzle. However, pressure drops to atmospheric pressure as the material comes out of the nozzle and is deposited, contrary to *e.g.* injection molding or compression molding where pressure is maintained until the end of the cycle. Thus, compaction pressure, which is present during more traditional polymer processing methods, is absent in ME-AM. As a consequence, this may influence intimate contact between strands and, therefore, may be more important than currently recognized, as was mentioned by Hart *et al.* [47]. This is also supported by the knowledge that strength development during thermoplastic welding has been shown to be pressure sensitive [48, 47].

Taking into account the previous four aspects, at the end of a ME-AM build cycle a component has an enormous heterogeneous mechanical property distribution along the component geometry. Locally, every material element has experienced different temperature, strain and shear rate, and pressure profiles leading to a variety of different microscopic structures and thermodynamic states. As a consequence, every material element has different intrinsic deformation behavior [19]. These differences in distribution of the mechanical properties will lead to certain macroscopic deformation behavior as measured in macroscopic tests, such as *e.g.* uniaxial tensile, uniaxial compression, torsional, 3-point bending, or impact tests.

Varying ME-AM processing parameters will generate different mechanical property distributions in a component. As a consequence, lots of disperse results have been reported in literature. These range from very low values for yield stresses [49, 50, 51, 9], to values similar to or near injection molding and compression molding components [49, 52, 53, 9, 10], and even improved properties with respect to components produced with conventional polymer fabrication processes [51, 10, 54].

Besides, polymers are viscoelastic materials. This type of behavior manifests itself in the initial intrinsic stress-strain behavior up to yield [55, 56] and the strain rate dependence of the yield stress and yield drop [57, 58, 59, 60, 61, 62]. The current study will focus on the influence that some of the printing parameters have on the macroscopic viscoelastic behavior of ME-AM components, in general, and, more specifically, the strain-rate dependence of Poly(Lactic Acid). As was previously demonstrated, the short-term strain-rate dependence has a direct relation to long-term behavior, such as creep and fatigue [63, 64, 65, 66, 67]. Therefore, this is crucial information for quantitatively predicting failure performance of ME-AM products via modeling and simulations.

However, only very few scientific contributions measure the effect of, for example, strain rate on the mechanical properties of ME-AM products. One of the first to measure this dependence was Rodriguez *et al.* [12] on ABS material processed on a

4

Stratasys machine. Only recently, and more than a decade later, this was also performed by Vairis *et al.* [68], also using an ABS material and FDM technology. Yet, these last authors applied a rather narrow strain rate range of less than one decade for their measurements. Furthermore, they did not relate their findings to an Eyring or Ree-Eyring

140 rate equation [57, 58], although it has been shown over the years by various research groups that an Eyring-type flow rule [57, 58, 60] describes accurately the visco-elastic strain-rate dependence of polymer molecules, incorporating it in accurate constitutive models for polymer materials [69, 70, 71, 72].

As far as the author's know, Bustillos *et al.* [36] and Song *et al.* [10] are the only

145 ones who have measured strain-rate sensitivity for ME-AM components made of PLA material. Bustillos *et al.* [36] measured it using creep experiments in a strain-rate range just over three decades and showed it on a $\log \sigma - \log \dot{\varepsilon}$ plot. Notwithstanding, they only determined strain-rate sensitivity for a range of just over one decade, without taking an Eyring rate equation into account. Furthermore, only one set of printing

150 parameters was used for each material. Song *et al.* [10] measured the influence of the infill orientation angle, but only performed measurements over a single decade and they neither used Eyring's rate equation.

The objective of the present study is to quantify and analyze the effect that several printing parameters have on the strain-rate dependence of ME-AM tensile test samples

155 produced with PLA material. An initial set of processing parameters is adopted that give mechanical properties near compression molding samples, which are fabricated using the same material. The compression molding technique is applied in order to get samples where orientation and stretch of the molecular chains is minimal, *i.e.* isotropic material behavior, which can not always be obtained with injection molded specimen

160 [73, 17, 18]. In this way, ME-AM results can directly be compared to bulk properties obtained from compression molded samples. ME-AM processing parameters that are changed are the infill velocity, the infill orientation angle, and the bed temperature. The lower bed temperature is well below T_g, while the higher bed temperature is near T_g. As such, the influence of molecular mobility can be accounted for, which will be more

165 enhanced closer to and above T_g. Finally, the ability of the Eyring flow rule to predict the yield stress in uniaxial tension is evaluated.

2. Materials and Methods

2.1. Material

The material used for the present study is a commercially available natural trans-

170 parent Polylactide (PLA) filament (Orbi-Tech, Leichlingen, Germany) with a nominal diameter of $1.75\ mm$ and a specific gravity of $1.25\ g\ cm^{-3}$. Recommended nozzle and bed temperatures range from $195\ ^\circ C$ to $240\ ^\circ C$ and from $40\ ^\circ C$ to $60\ ^\circ C$, respectively. All samples were fabricated from a single spool, and the filament was used as-received.

2.2. Material processing

175 Tensile samples were manufactured on an open-source RepRap Sirius 3D printer (Moebyus Machines, Madrid, Spain) using a $0.4\ mm$ nozzle size. Sample dimensions are given in Figure 1(a). This tensile test specimen is based on specimen type 1BA

5

according to the ISO 527-2 norm, but adapted to avoid fracture in the fillet. The dimensions are chosen to be able to machine them from the compression molded square plates (see next section).
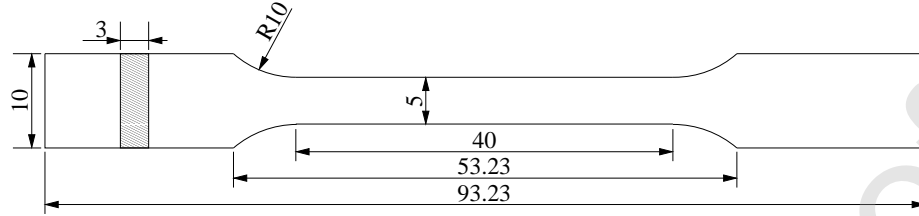
(a)
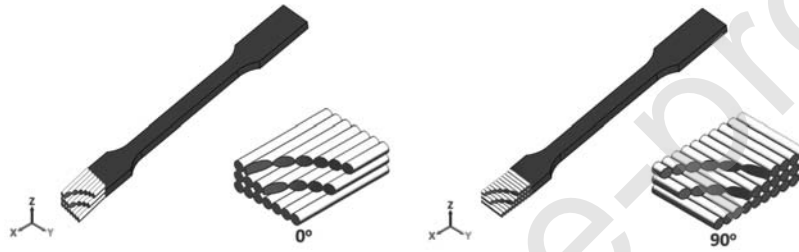
(b)

Figure 1: *(a)* Tensile test specimen dimensions in mm. *(b)* Schematic of infill orientation angle.

Starting from an STL-file of the tensile sample, the Simplify3D slicing software was used to generate the G-code file that can be handled by the Sirius ME-AM machine. Processing parameters that were used unaltered to produce all ME-AM tensile samples are given in Table 1. Furthermore, 3 printing parameters are changed each at two levels, thus leading to 8 different sets, to investigate their influence on the resulting mechanical properties: (i) print velocity; (ii) infill orientation angle; (iii) bed temperature. These levels are given in Table 2 and a schematic of the infill orientations is also given in Figure 1(b). For each of the 8 sets, 18 equal samples were distributed on the printer's XY plane (*i.e.* the printer's bed) and manufactured using a single G-code file.

2.3. Compression molding

Square plates with dimensions of $100 \times 100 \times 3 \ mm^3$ were compression molded in a hot press. Approximately $45 \ gr$ of chopped filament strands were preheated in the mold at $210 \ °C$ for $15 \ min$ and subsequently compressed in successive steps of increasing force during $5 \ min$, allowing degassing by releasing pressure between steps. Next, cooling to room temperature was established by placing the mold into a cold press at moderate force during several minutes. From these square plates, tensile test samples were machined with the dimensions as given in Figure 1(a).

2.4. Mechanical characterization

Uniaxial tensile tests were performed on a MTS Criterion C43.104 universal test system with a $10 \ kN$ load cell. All experiments were measured at room tempera-

6

Table 1: Processing parameters used to manufacture *all* ME-AM tensile samples.

Processing parameter	Value
Nozzle diameter [mm]	0.40
Extrusion width [mm]	0.30
Layer height [mm]	0.20
Number of perimeters	2
Fill percentage	100%
Outline overlap	80%
Extrusion temperature [$^\circ C$]	200

Table 2: Levels of processing parameters used to manufacture different sets of ME-AM tensile samples.

Processing parameter	Low value	High value
Printing speed v_p [$mm\ s^{-1}$]	9	35
Infill orientation angle α_{or}	0°	90°
Bed temperature T_b [$^\circ C$]	50	60

ture (23 $^\circ C$). Constant linear strain rates were applied in the range from $10^{-5}\ s^{-1}$ to $10^{-1}\ s^{-1}$. At least three samples, and generally five samples, were used for every single strain rate. As is common for polymers, the maximum stress value in the engineering stress-strain curves is considered as the polymer's yield stress. Conversion from engineering to true yield stresses was accomplished by assuming that the material volume remains constant during uniaxial tensile testing [74, 75].

2.5. Apparent density

Due to the fact that ME-AM parts generally have interstitial voids, its mechanical properties are affected by this voided structure. To compensate for this and provide a more fair comparison of the material behavior, the apparent densities of the resulting ME-AM samples were determined. Both mass and external volume were measured for every single sample to calculate the apparent density:

$$\rho_{app} = \frac{m_{sample}}{V_{sample}} .$$ (1)

Furthermore, an approximation of the porosity of the samples (in percentage) was determined by using the material density as given by the filament provider, *i.e.* $\rho_{PLA} = 1.25\ g\ cm^{-3}$:

$$\text{Porosity} = \frac{\rho_{PLA} - \rho_{app}}{\rho_{PLA}} .$$ (2)

7

2.6. Thermal analysis

Differential Scanning Calorimetry (DSC) was performed on a NETZSCH DSC 214 *Polyma* apparatus. Portions of filament, and compression molded and fabricated ME-AM samples were subjected to a heating-cooling-heating sequence under nitrogen at a scanning rate of $10 \ K \ min^{-1}$ and isothermal periods of $5 \ min$. Crystallinity χ_c was calculated using the following equation:

$$\chi_c = \frac{\Delta H_m - \Delta H_c}{\Delta H_m^0} \ , \tag{3}$$

where ΔH_m, ΔH_c, and ΔH_m^0 are the melting enthalpy, the crystallization enthalpy and the melting enthalpy of pure crystalline PLA, respectively. The value for 100% crystalline PLA was taken to be $\Delta H_m^0 = 93.7 \ J \ g^{-1}$ [76].

3. Modeling

It has been often demonstrated, that the deformation kinetics of polymers can be characterized by a linear dependence of the yield stress on both the logarithm of strain rate as well as the temperature [74, 60, 77, 66]. Typically, a polymer's yield stress also depends on pressure [78, 79], particularly evident in testing under hydrostatic pressure [80, 81, 82, 83] or by the yield stress difference under tensile and compression loading [77, 79]. However, this study only focuses on tensile tests, so that part is omitted here.

If in the measured strain rate and temperature range, the polymer shows a thermorheologically simple response [60], *i.e.* the deformation response is governed only by a single molecular deformation process, the deformation kinetics of the yield stress can be accurately described by an Eyring-type flow equation:

$$\dot{\varepsilon}(\sigma, T) = \dot{\varepsilon}_0 \exp\left(-\frac{\Delta U}{RT}\right) \sinh\left(\frac{\sigma_y V^*}{kT}\right) \ . \tag{4}$$

Here, $\dot{\varepsilon}$ is the uniaxially applied strain rate, $\dot{\varepsilon}_0$ a rate constant, ΔU the activation energy ($184 \ kJ \ mol^{-1}$, as taken from literature [66]), R the universal gas constant ($8.314472 \ J \ mol^{-1} \ K^{-1}$), T the absolute temperature in K, σ_y is the yield stress, V^* the activation volume, and k is the Boltzmann's constant ($1.38054 \cdot 10^{-23} \ J \ K^{-1}$). If written in terms of the yield stress as a function of strain rate, the equation becomes:

$$\sigma_y(\dot{\varepsilon}, T) = \frac{k \, T}{V^*} \sinh^{-1}\left[\frac{\dot{\varepsilon}}{\dot{\varepsilon}_0 \exp\left(-\frac{\Delta U}{RT}\right)}\right] \ . \tag{5}$$

At the yield stress, where $\sigma_y > kT/V^*$ and thus $\sinh(x) = \frac{1}{2}\left[\exp(x) - \exp(-x)\right] \approx \frac{1}{2}\exp(x)$, Equation 4 can be rewritten as:

$$\sigma_y(\dot{\varepsilon}, T) = \frac{k \, T}{V^*}\left[\ln\left(\frac{2\dot{\varepsilon}}{\dot{\varepsilon}_0}\right) + \frac{\Delta U}{RT}\right] \ . \tag{6}$$

However, many polymers show thermorheologically complex behavior, manifested by a change in the slope in the yield stress vs. logarithmic strain-rate plots [74]. In

8

these cases, two molecular deformation processes govern the yield kinetics, often indicated by an α- and a β-relaxation process. Assuming that these two processes act independently and in parallel, the yield kinetics can be described by the Ree-Eyring modification [58] of the Eyring [57] flow rule:

$$\sigma_y = \sigma_\alpha + \sigma_\beta = \frac{k\,T}{V_\alpha^*} \sinh^{-1}\left[\frac{\dot{\varepsilon}}{\dot{\varepsilon}_{0,\alpha}\exp\left(-\frac{\Delta U_\alpha}{RT}\right)}\right] + \frac{k\,T}{V_\beta^*} \sinh^{-1}\left[\frac{\dot{\varepsilon}}{\dot{\varepsilon}_{0,\beta}\exp\left(-\frac{\Delta U_\beta}{RT}\right)}\right].$$
(7)

Note that true stress values are referred to in these equations.

For the case of PLA, it has been shown that the yield kinetics contain contributions of two molecular deformation processes ($\alpha + \beta$) [62]. By measuring the strain-rate and temperature dependence in uniaxial compression tests, both upper-yield as well as lower-yield stresses could be determined. While lower-yield stress only manifested an α-contribution, upper-yield stress was controlled by both the α- and β-processes [66, 62]. In uniaxial tensile tests, which are applied in the current paper, only the upper-yield stress can be determined. In these tests, from the yield stress on, strain localization phenomena occur such as crazing (amorphous regions) and shear-yielding (crystalline regions) leading to failure [32] and impeding the determination of the lower-yield stress. Hence, in tensile, separation of the two molecular processes can not always be easily determined. In such cases, Equation 7 can be written as:

$$\sigma_y = \frac{k\,T}{V_{\alpha+\beta}^*} \sinh^{-1}\left[\frac{\dot{\varepsilon}}{\dot{\varepsilon}_{0,\alpha+\beta}\exp\left(-\frac{\Delta U_{\alpha+\beta}}{RT}\right)}\right].$$
(8)

Note that this is implicitly the same equation as Equation 5. Nonetheless, the activation volume, the rate constant, and the activation energy of Equation 8 incorporate the contributions of the two molecular processes instead of only a single process as in Equation 5.

4. Results and Discussion

For this section, the nomenclature as follows is used to indicate the samples which are fabricated via the different processing methods and parameters. The compression molded samples are indicated with *CM*. On the other hand, the Material Extrusion Additive Manufactured samples are indicated by letters and numbers in the following order: the printing *v*elocity in $mm\,s^{-1}$, infill *o*rientation angle, and bed *T*emperature in $^\circ C$. For example, sample *v35o0T50* is a ME-AM sample printed at a velocity of $v_p = 35\,mm\,s^{-1}$, an infill orientation angle of $\alpha_{or} = 0^\circ$, and a bed temperature of $T_b = 50\,^\circ C$.

First, DSC data will be analyzed in order to gain knowledge about characteristic material transition temperatures and crystallinities. Second, the *CM* samples will be looked at, as these samples are more isotropic since no preferential orientation and stretch of the molecular chains is present. These samples are considered to show the "fingerprint" behavior and bulk properties of the base material. Last, ME-AM samples

9

will be considered and compared with each other and with the *CM* samples, taking influences such as processing parameters and interstitial voids into account.

240   *4.1. Thermal analysis*

Figure 2 shows the DSC curves for the as-received PLA filament, a *CM* sample, and a ME-AM sample (*v9o0T50*). For the DSC thermographs of the first heating cycle, a glass transition temperature of around $T_g = 66\ °C$ was detected. During the second heating cycle, all samples showed $T_g = 61\ °C$. This PLA material is able to crystallize, 245   as cold crystallization can be observed between $95 - 145\ °C$ with a peak temperature at approximately $T_c = 122\ °C$. It is directly followed by melting $(145 - 165\ °C)$ at a peak temperature of $T_m = 152\ °C$. These characteristic temperatures are very similar to the ones reported by Carrasco *et al.* [84] and by Srinivas *et al.* [25] for PLLA with a D content of approximately 4%. It is assumed that the PLA used in this study has 250   therefore a similar composition (this could, however, not be confirmed).
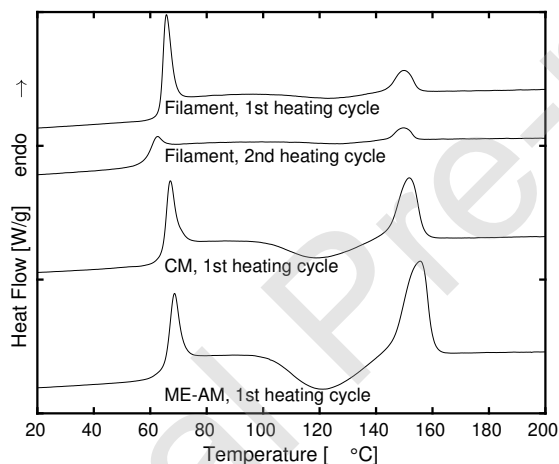
Figure 2: Different DSC curves for PLA material used in present study: 1st heating of as-received filament; 2nd heating of as-received filament after controlled cooling; 1st heating of *CM* sample; 1st heating of ME-AM sample.

The calculated crystallinity detected for the as-received filament during the first heating cycle was equal to $\chi_c = 1.2\%$. The ME-AM sample also shows an area for cold crystallization and melting that have approximately the same magnitude, resulting in a crystallinity of $\chi_c = 0.8\%$. In Figure 2, the *CM* sample shows the highest crystallinity, 255   although still at a low value of $\chi_c = 1.7\%$. During the DSC cooling cycle, none of the samples demonstrated crystallization. Merely a glass transition temperature of around $T_g = 55\ °C$ was observed for all samples. This indicates a low ability to crystallize of the employed PLA during cooling [84]. All samples showed the same thermographs for the second heating cycle with crystallinities below 0.6%. Not all ME-AM sample 260   sets were submitted to DSC thermographs. However, the ME-AM samples for which DSC curves were obtained, all showed low crystallinity values less than 2%.

10

Srinivas *et al.* [25] also showed that no crystallization occurred during the ME-AM process for their material. Their DSC curves showed a deviation from the baseline for cold crystallization at around 95 °C and a peak value of approximately $T_c = 110$ °C.

265 Here, deviation from the base line for cold crystallization starts from around 95 °C, but the peak temperature is even higher, *i.e.* $T_c = 122$ °C, making it even more difficult to crystallize. Therefore, although it is not checked for all ME-AM samples, it is assumed that negligible crystallization occurs during the ME-AM process and that it will not have a significant effect on the mechanical properties.

270 *4.2. Compression molding*

The mechanical characterization results for the *CM* samples are given in Figure 3 and Table 3. The *CM* samples show brittle behavior (see Figure 3(a)), as is to be expected for PLA in uniaxial tensile tests [32]. This is due to the very large strain softening response right after yield followed by the weak strain hardening [66, 62],

275 which to a large extend determines the toughness of a material.

As can be seen from 3(b), the strain-rate dependence of the yield stress is adequately captured with a single molecular deformation process, showing a high coefficient of determination R^2 close to unity. However, as was shown by Van Breemen *et al.* [62], PLA has thermorheologically complex behavior that was well described with

280 2 molecular deformation processes, one visible in the strain-rate dependent behavior of the lower yield stress and the two processes combined in the upper yield stress during uniaxial compression tests.

Here, the experimental data can be described by Equation 8 with a combined activation volume and rate constant of $V^*_{\alpha+\beta} = 1.05$ nm^3 and $\dot{\varepsilon}_{0,\alpha+\beta} = 5.38 \cdot 10^{22}$ s^{-1},

285 respectively, giving a slope of 8.9 MPa/decade. It is explicitly mentioned that the combined activation energy is taken equal to the activation energy as determined by Engels *et al.* [66], *i.e.* $\Delta U_{\alpha+\beta} = 184$ kJ mol^{-1}. The activation volume determined here is higher than the one given by Engels *et al.* [66], who measured (similar to Van Breemen *et al.* [62]) a slope of ± 13.5 MPa/decade. This can be explained in two ways: (i) a
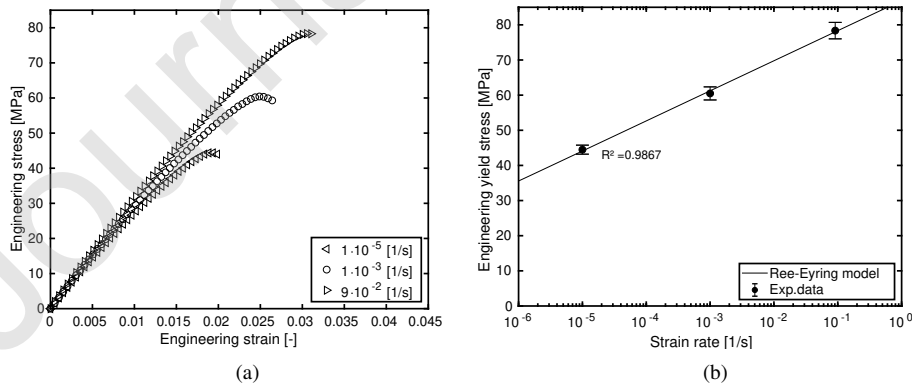
Figure 3: Engineering stress/strain response of *CM* samples. *(a)* Stress as a function of strain. *(b)* Yield stress as a function of logarithmic strain rate. Symbols are experimental results, solid line is a model prediction.

11

290 different grade PLA is used; (ii) Engels *et al.* [66] measured in compression, which is known to give higher slopes and stresses compared to uniaxial tensile tests [77, 85].

From Figure 3 and Table 3, other viscoelastic effects can be detected, such as a slightly increasing elastic modulus E (between 3.0 GPa and 3.5 GPa) and increasing strain at yield ε_y (from $\pm 2\%$ to $\pm 3\%$) for increasing strain rates $\dot{\varepsilon}$. Additionally, brit-
295 tleness can be established by the small difference between strain at yield ε_y and strain at break ε_b (see Table 3).

Table 3: Measured engineering mechanical properties for *CM* and ME-AM samples.

Sample nomenclature	$\dot{\varepsilon}$ $[s^{-1}]$	E [MPa]	σ_y [MPa]	ε_y [%]	ε_b [%]
CM	$1 \cdot 10^{-5}$	2994 ± 190	44.49 ± 1.28	1.91 ± 0.16	1.99 ± 0.25
	$1 \cdot 10^{-3}$	3135 ± 99	60.49 ± 1.86	2.50 ± 0.05	2.64 ± 0.12
	$9 \cdot 10^{-2}$	3461 ± 173	78.36 ± 2.34	3.06 ± 0.05	3.10 ± 0.04
v35o0T50	$1 \cdot 10^{-5}$	3022 ± 57	47.58 ± 0.89	2.45 ± 0.13	2.60 ± 0.24
	$1 \cdot 10^{-3}$	3108 ± 39	62.76 ± 0.35	2.62 ± 0.04	3.43 ± 0.78
	$9 \cdot 10^{-2}$	3127 ± 32	75.01 ± 1.01	3.34 ± 0.15	3.51 ± 0.12
v9o0T50	$1 \cdot 10^{-5}$	3062 ± 35	45.54 ± 1.07	1.94 ± 0.09	1.95 ± 0.09
	$1 \cdot 10^{-3}$	3184 ± 13	60.36 ± 0.38	2.52 ± 0.06	2.55 ± 0.07
	$9 \cdot 10^{-2}$	3157 ± 81	73.15 ± 1.00	2.95 ± 0.10	2.96 ± 0.10
v35o0T60	$1 \cdot 10^{-5}$	3310 ± 84	48.44 ± 1.25	2.06 ± 0.03	2.95 ± 0.40
	$1 \cdot 10^{-3}$	3306 ± 32	62.10 ± 1.04	2.37 ± 0.03	4.44 ± 1.91
	$9 \cdot 10^{-2}$	3265 ± 41	74.65 ± 0.42	2.85 ± 0.03	3.24 ± 0.34
v9o0T60	$1 \cdot 10^{-5}$	3376 ± 109	49.11 ± 0.98	1.99 ± 0.03	2.14 ± 0.15
	$1 \cdot 10^{-3}$	3290 ± 35	62.04 ± 0.80	2.35 ± 0.04	3.73 ± 0.52
	$9 \cdot 10^{-2}$	3276 ± 37	75.01 ± 0.53	2.83 ± 0.01	3.76 ± 0.26
v35o90T50	$1 \cdot 10^{-5}$	3061 ± 49	48.29 ± 1.09	2.22 ± 0.03	2.63 ± 0.17
	$1 \cdot 10^{-3}$	3269 ± 32	60.78 ± 0.55	2.39 ± 0.03	3.92 ± 0.19
	$9 \cdot 10^{-2}$	3261 ± 99	72.74 ± 0.69	2.87 ± 0.08	4.22 ± 0.43
v9o90T50	$1 \cdot 10^{-5}$	3078 ± 84	44.92 ± 0.26	1.94 ± 0.04	1.95 ± 0.04
	$1 \cdot 10^{-3}$	3174 ± 52	55.61 ± 1.01	2.25 ± 0.03	2.33 ± 0.06
	$9 \cdot 10^{-2}$	3220 ± 43	69.80 ± 1.18	2.83 ± 0.04	3.11 ± 0.27
v35o90T60	$1 \cdot 10^{-5}$	3184 ± 134	44.73 ± 1.11	1.93 ± 0.02	2.22 ± 0.27
	$1 \cdot 10^{-3}$	3232 ± 42	55.57 ± 0.56	2.17 ± 0.02	2.81 ± 0.41
	$9 \cdot 10^{-2}$	3235 ± 99	69.17 ± 0.77	2.73 ± 0.04	3.51 ± 0.42
v9o90T60	$1 \cdot 10^{-5}$	3175 ± 65	46.94 ± 1.42	1.98 ± 0.03	2.03 ± 0.06
	$1 \cdot 10^{-3}$	3158 ± 30	58.67 ± 0.49	2.33 ± 0.04	2.57 ± 0.11
	$9 \cdot 10^{-2}$	3206 ± 37	72.13 ± 1.15	2.84 ± 0.02	3.26 ± 0.12

12

4.3. Material extrusion additive manufacturing

While the mechanical properties of compression molded samples is generally only determined by crystallinity (negligible in this case) and by the thermodynamic state
300 of the amorphous phase [33, 72], in the case of ME-AM samples an additional aspect arises that has its influence as well: the orientation and stretch of molecular chains [38, 35, 7]. These are all affected by the thermo-mechanical history the material has experienced, *i.e.* the shear rate $\dot{\gamma}(t)$ and temperature $T(t)$ as a function of time t. Furthermore, these aspects also have crossover effects.

305 Results for the *v35o0T60* sample set is shown in Figure 4, and Table 3 gives the numerical values. This set has an apparent density of $1.21\ g\ cm^{-3}$ (compared to a material density of $1.25\ g\ cm^{-3}$), leading to an approximate average porosity of 3.5%. This particular set is shown to highlight some distinct features between *CM* and ME-AM samples.

310 In order to determine what the effect of the different printing parameters on the material behavior is and compare the *CM* and ME-AM samples in a macroscopic sense, a compensation of the voided structure of ME-AM samples is applied. The yield stresses of ME-AM samples can be corrected for to represent "solid" samples, using the apparent density and the material density given by the filament manufacturer. Figure 4(b)
315 shows these *volume corrected* results. In the remainder of the paper, if different sets of ME-AM samples are compared with each other, the volume corrected yield stresses will be shown, unless stated otherwise.
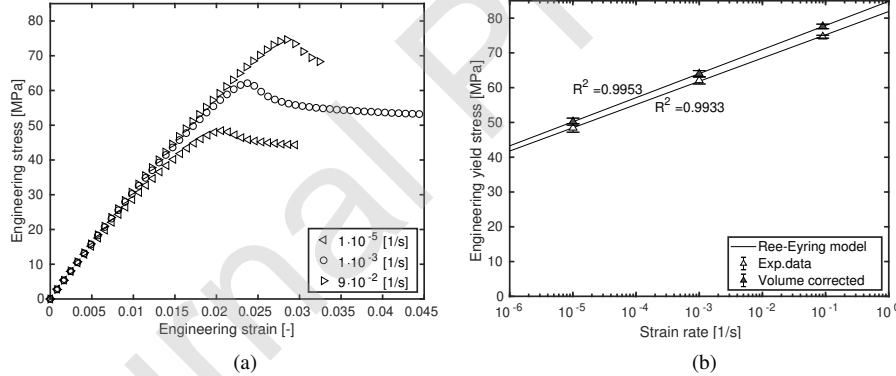
Figure 4: Engineering stress/strain response of v35o0T60 samples. *(a)* Stress as a function of strain. *(b)* Yield stress and volume corrected yield stress as a function of logarithmic strain rate. Symbols are experimental results, solid lines are model predictions.

Similar to the *CM* sample set, the strain-rate dependence of the yield stress is adequately captured with a single molecular deformation process. The yield stress data can
320 be described with a combined activation volume and rate constant of $V^*_{\alpha+\beta} = 1.30\ nm^3$ and $\dot{\varepsilon}_{0,\alpha+\beta} = 4.62 \cdot 10^{20}\ s^{-1}$, respectively, giving a slope of 7.2 MPa/decade. The coefficient of determination R^2 is very close to unity, and improves for the volume corrected results, showing that an Eyring-type flow equation can give an excellent description of the yield data. With reference to the improvement of the coefficient of

13

325 determination by representing "solid" samples, that is a trend seen for all ME-AM sample sets.

Two aspects immediately draw the attention if the *CM* results are compared to the *v35o0T60* samples. First, the slope of the strain-rate dependence for the *v35o0T60* set is significantly lower than for the *CM* samples. Second, these ME-AM samples behave

330 semi-ductile instead of brittle (*i.e.* compare Figure 3(a) with Figure 4(a)). These are clear effects related to the processing phase, and possible explanations will be given later on.

Equal to the *CM* samples, the strain at yield increases (from $\pm 2\%$ to $\pm 3\%$) for increasing strain rates. However, the viscoelastic effect on the elastic modulus is absent

335 in this ME-AM sample set, as it remains approximately constant at 3.3 GPa. Furthermore, polymer materials generally show an almost constant or slightly increasing strain at break when characterized at augmenting strain rates [86, 87, 88]. Although dispersion of the strain at break ε_b for polymers is generally high, this previous trend is not seen here (see Table 3), nor in several of the other ME-AM sample sets. This can also

340 be observed in the measurements by Rodriguez *et al.* [12] for their ME-AM samples of ABS material (see Figure 14 of their paper). At this moment, no plausible explanation can be given for this observation. It may be related to the position of the sample on the printing bed. This could not be confirmed and additional research will be necessary to clarify this phenomenon. That is, however, out of the scope of the present study.

345 *4.4. Anisotropic yielding*

As seen by comparing Figures 4(b) and 3(b), the processing phase clearly has an influence on the macroscopic material behavior. To further establish how anisotropy in ME-AM samples due to the infill orientation (as reported previously by other research groups [12, 20, 11]) is affecting strain-rate dependence, *CM* samples are compared to

350 ME-AM samples that are printed at both $\alpha_{or} = 0°$ and $\alpha_{or} = 90°$. Figure 5 shows the volume corrected yield stresses σ_y as a function of logarithmic strain rate $\dot{\varepsilon}$ for *CM*, *v35o0T50*, and *v35o90T50* samples.

The dashed lines in Figure 5 indicate that all three samples clearly have different slopes. Thus, anisotropic effects are also visible in the strain-rate dependence of

355 ME-AM components, as was to be expected based on research of anisotropic effects in injection molding samples [17, 18]. Additionally, it turns out that there is also a difference of strain-rate effect between isotropic samples (*CM*) and anisotropic samples (*v35o0T50* or *v35o90T50*). This effect, as far as the authors know, has not been reported before.

360 Three different slopes may indicate three distinct molecular deformation processes [89]. However, up-to-date only two processes have been reported thus far for PLA [90, 62]. Since no third process has been reported previously, it is assumed that only two molecular processes are present ($\alpha + \beta$). As experiments have only been performed at room temperature, activation energies for the two processes are taken from literature

365 [62]: $\Delta U_a = 480 \ kJ \ mol^{-1}$ and $\Delta U_b = 100 \ kJ \ mol^{-1}$.

Next, it is also observed that all ME-AM sample sets printed at an infill orientation of $\alpha_{or} = 90°$ approximately have the same slope in the lower measured strain rate range, *i.e.* $\dot{\varepsilon} = 10^{-5} - 10^{-3}$. As mentioned before, that slope is significantly less

14
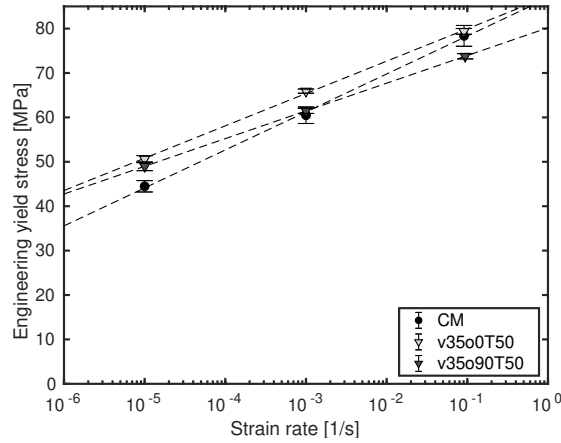
Figure 5: Volume corrected engineering yield stress as a function of logarithmic strain rate for *CM* (●), v35o0T50 (▽), and v35o90T50 (▼) samples. Symbols are experimental results, lines are a guide to the eye.

steep than the slope measured for the *CM* sample set. As a consequence, it is assumed
370 that at the lower measured strain rate range for ME-AM samples printed at $\alpha_{or} = 90°$, the yield stress is controlled by the α-process only. Accordingly, and based on the observations of Van Breemen *et al.* [62], the yield stress of the *CM* samples presumably contains contributions of both processes ($\alpha + \beta$).

Last, and following the research on anisotropic yielding in oriented polypropylene
375 and polyethylene [91, 17, 18], it is assumed that the yield stress measurements of the ME-AM sample sets printed at $\alpha_{or} = 90°$ represent the reference yield kinetics of the α-relaxation process. The enhanced slope observed for ME-AM samples printed at $\alpha_{or} = 0°$ is then thought to be a contribution of the molecular orientation and stretch due to the printing process.

380 To assess if orientation and stretch during the ME-AM process is actually occurring, a qualitative macroscopic measurement procedure is applied based on thermal shrinkage. This procedure is similar to what has been used by Rodriguez *et al* [12]. ME-AM test specimen are heated in an oven above the glass transition temperature

Table 4: Average dimensional changes and crystallinity of ME-AM sample sets after a thermal treatment at $100 \,°C$ for six hours. Expansion: $+$; Contraction: $-$.

Sample nomenclature	Length [%]	Width [%]	Height [%]	Crystallinity [%]
v9o0T50	−2.8	−0.9	+5.0	39.1
v9o90T50	−1.3	−0.7	+1.5	39.4
v35o0T50	−9.3	+1.1	+9.0	37.2
v35o90T50	−1.9	−2.7	+4.9	37.4

15

($T_g = 66\ °C$) and below the crystallization temperature ($T_c = 122\ °C$). After mea-
385 suring sample dimensions at room temperature, the specimens were placed in an oven
at $100\ °C$ for six hours. Next, the samples were cooled to room temperature and sam-
ple dimensions were measured again. Expansion($+$)/contraction($-$) percentages were
then determined from the dimensional differences. Three samples for each measured
set were used to determine these dimensional changes. Results are reported in Table 4.

390 In order to determine to what extent cold crystallization affects the dimensional
shrinkage, DSC measurements were performed on thermal treated test specimen. All
DSC thermographs had the same form showing solely a melting peak with a shoulder
between $110 - 165\ °C$ and its peak temperature at $T_m = 150\ °C$. This resulted
for all samples measured in similar crystallinities around 38%. Samples fabricated at
395 a printing velocity of $v_p = 9\ mm\ s^{-1}$ showed a slightly higher crystallinity, while
samples at $v_p = 35\ mm\ s^{-1}$ had crystallinities closer to 37%, irrespective of the
printing direction (see Table 4).

It can be seen that all sample sets demonstrate dimensional contraction in the di-
rection of the strands, *i.e.* a length shrinkage for $\alpha_{or} = 0°$ and width contraction for
400 $\alpha_{or} = 90°$. Furthermore, all sample sets show an increase of the height dimensions af-
ter the thermal treatment, which is the direction perpendicular to the strand deposition.

From the DSC measurements, it is clear that crystallization affects these dimen-
sional changes. However, if the dimensional changes are only due to crystallization and
the material contracts more in the strand direction than perpendicular to it, the samples
405 at $\alpha_{or} = 0°$ would contract in a similar manner, irrespective of the printing velocity,
since crystallinity values are similar. In fact, the samples at $v_p = 9\ mm\ s^{-1}$ would
have to contract slightly more, due to a somewhat higher crystallinity. Furthermore, all
directions would show contraction and no expansion. Therefore, it is concluded that
the differences in dimensional changes at different printing velocities are not only due
410 to crystallization, but also because of relaxation of the molecular chain orientation and
stretch.

It is suggested that crystallization has a comparable effect on all samples, and that
the differences in dimensional changes are indicative to the degree of the molecular
chain orientation and stretch [12]. A higher dimensional change then indicates a higher
415 molecular orientation and stretch in that direction, *i.e.* the strand direction.

The thermal treatment results imply that orientation and stretch is substantially
higher (more than 3 times) at the higher printing velocity, both for $\alpha_{or} = 0°$ as well as
$\alpha_{or} = 90°$. For sample set *v35o0T50*, the results manifest a strong contraction in the
length direction, combined with an expansion in both the height *and* width dimension.
420 This again suggests that the differences in dimensional changes are due to relaxation
of the molecular chain orientation and stretch.

Taking these considerations into account, the Ree-Eyring parameters can be deter-
mined for all measured sets. Based on the *volume corrected* true yield stresses, the
values of these parameters are given in Table 5 in order to describe the yield stress with
425 Equation 7. The average apparent density and resulting approximate porosities are also
given in Table 5.

As can be observed in Table 5, it is assumed that the activation volume of the β-
relaxation process is not influenced by the printing process, *i.e.* the orientation and
stretch of the molecular chains. This, of course, is not confirmed experimentally. One

16

Table 5: Average apparent density, porosity, and model parameters used to describe the yield behavior of Compression Molded (*CM*) and ME-AM samples. Activation energies are taken as $\Delta U_a = 480 \ kJ \ mol^{-1}$ and $\Delta U_b = 100 \ kJ \ mol^{-1}$ [62].

Sample nomenclature	$\bar{\rho}_{app}$ [$g \ cm^{-3}$]	Porosity [%]	V_α^* [nm^3]	$\dot{\varepsilon}_{0,\alpha}$ [s^{-1}]	V_β^* [nm^3]	$\dot{\varepsilon}_{0,\beta}$ [s^{-1}]
CM	1.25	0	1.52	$2.20 \cdot 10^{73}$	3.40	$3.40 \cdot 10^{11}$
v35o0T50	1.18 ± 0.013	5.5 ± 1.0	1.23	$1.49 \cdot 10^{73}$	3.40	$2.10 \cdot 10^{19}$
v9o0T50	1.19 ± 0.009	4.8 ± 0.8	1.22	$4.10 \cdot 10^{73}$	3.40	$2.10 \cdot 10^{19}$
v35o0T60	1.21 ± 0.010	3.5 ± 0.8	1.30	$7.92 \cdot 10^{72}$	3.40	$2.10 \cdot 10^{19}$
v9o0T60	1.21 ± 0.011	3.1 ± 0.8	1.30	$7.59 \cdot 10^{72}$	3.40	$2.10 \cdot 10^{19}$
v35o90T50	1.23 ± 0.004	1.3 ± 0.3	1.52	$6.91 \cdot 10^{71}$	3.40	$4.60 \cdot 10^{16}$
v9o90T50	1.20 ± 0.005	3.6 ± 0.4	1.52	$2.41 \cdot 10^{72}$	3.40	$6.19 \cdot 10^{15}$
v35o90T60	1.22 ± 0.008	2.1 ± 0.6	1.52	$3.38 \cdot 10^{72}$	3.40	$1.60 \cdot 10^{16}$
v9o90T60	1.22 ± 0.006	2.1 ± 0.4	1.52	$1.21 \cdot 10^{72}$	3.40	$9.07 \cdot 10^{15}$

430 can also observe that the apparent density is generally higher for $\alpha_{or} = 90°$, and apparent density dispersion is lower. This is thought to be related to fact that less time passes between the deposition of adjacent strands, leading to a higher average temperature. As a consequence, material can flow more easily and porosity will be reduced.

435 The experimental engineering stress-strain curves for the ME-AM samples are shown in Figure 6, while the *volume corrected* engineering yield stress as a function of logarithmic strain rate are given in Figure 7. The Ree-Eyring model can adequately describe the experimental data, with coefficients of determination R^2 very close to unity for all cases.

440 Since the time between the deposition of adjacent strands for longitudinal ($0°$) and transverse ($90°$) specimens is not equal, the temperature profile over time for *e.g.* *v35o0T50* and *v35o90T50* samples will neither be equal [23]. This is additionally confirmed by the difference in approximate porosity between these two samples, which demonstrate the highest and lowest porosity, respectively. Thus, also because it is clear
445 that the printing parameters have a different effect on $0°$ and $90°$ oriented samples, their influence on the mechanical properties for these $0°$- and $90°$-samples will initially be treated separately.

4.5. Longitudinal printing direction: $\alpha_{or} = 0°$

In Figures 6(a) and 7(a) the effect of the printing velocity can be seen for a bed
450 temperature of $T_b = 50°C$. The printing velocity clearly influences ductility, improving for higher printing velocity. Furthermore, a higher printing velocity gives higher stresses. The activation volume, on the other hand, seems to be hardly affected by the printing velocity (see Table 5). Interestingly, the effect of the printing velocity disappears completely at the higher bed temperature of $T_b = 60°C$ (Figures 6(b) and 7(b)).

17
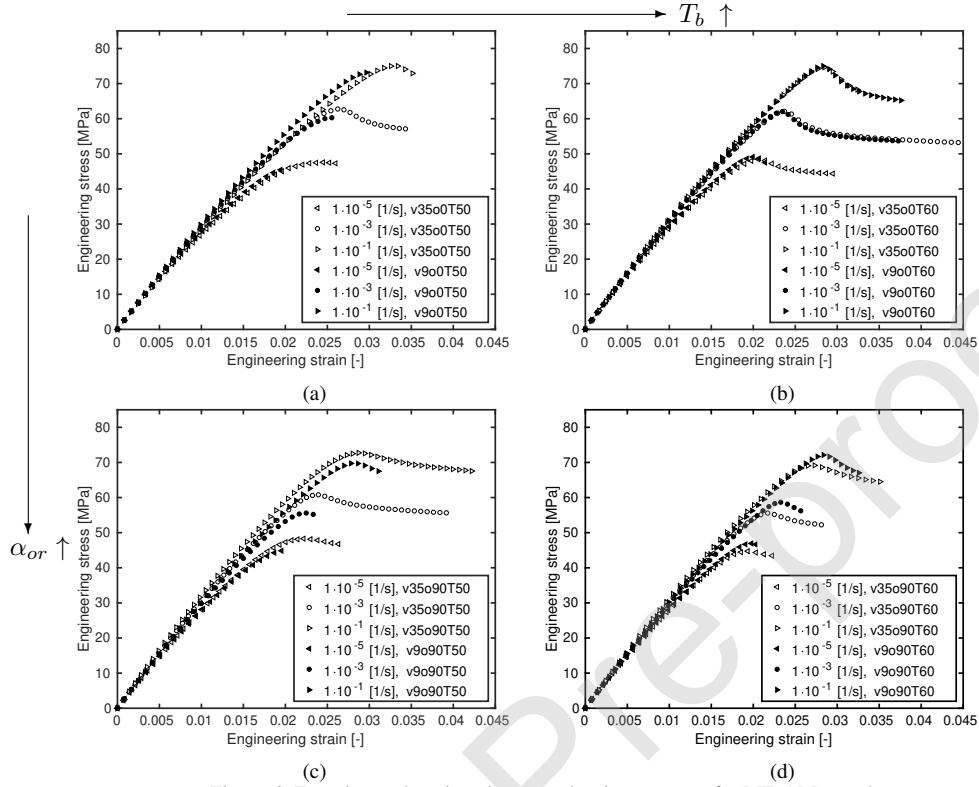
Figure 6: Experimental engineering stress/strain responses for ME-AM samples.

455   The effect of the bed temperature at a printing velocity of $v_p = 35\ mm\ s^{-1}$ can be determined by comparing the open symbols in Figures 6(a) and 6(b) and the triangular symbols in Figures 7(a) and 7(b). Results for bed temperature $T_b = 60°C$ show higher ductility and an increased elastic modulus E. At $T_b = 50°C$, the activation volume is somewhat higher (see also Table 5), manifested by a slightly increased dependence 460 on strain rate, which may be related to orientation [17, 18]. However, this difference almost completely disappears when the yield stress values are not compensated for porosity (not shown here). The same effects are seen for a printing velocity of $v_p = 9\ mm\ s^{-1}$ (*i.e.* closed symbols in Figure 6(a)/6(b); diamond and square symbols in Figure 7(a)/7(b)), except for the difference that the yield stress values for $T_b = 50°C$ 465 are lower.

    Based on findings by Senden *et al.* [92, 18], Van Erp *et al.* [91, 17], and Sun *et al.* [23], the results presented here are thought to be effects of a combination of the strain and temperature profiles the material experiences during ME-AM processing. And it is the combination of these two profiles that result in the complex, and sometimes 470 contrary, behavior observed.

    On the one hand, the strain profile leads to a certain amount of orientation and

18
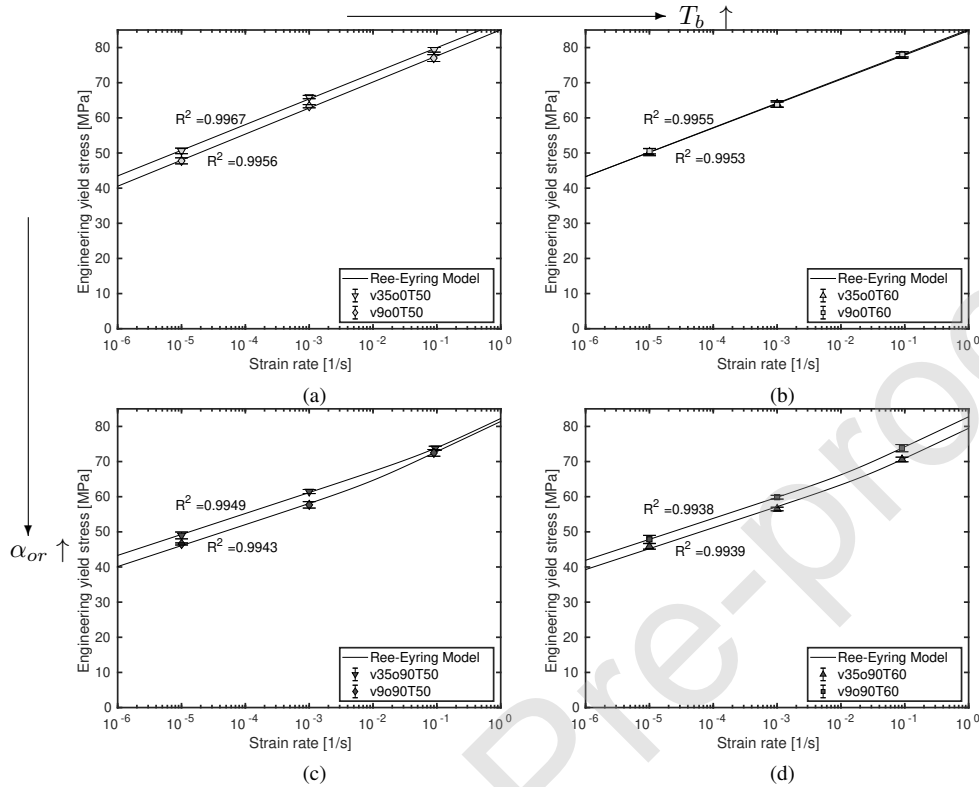
Figure 7: Volume corrected engineering yield stresses as a function of logarithmic strain rate for ME-AM samples. Symbols are experimental results, solid lines are model predictions.

stretch of the polymer chains. As observed, differences in stretch (*v35o0T50* vs. *v9o0T50*) hardly affects the slope of the strain-rate dependence, but does have an effect on the yield stress values. This seems to indicate that orientation in the tensile direction de-

475   termines the activation volume [17, 18], and that stretching of the polymer chains only influences the level of yield stress. Hence, this can be interpreted as a deformation dependence of the rate constant, as was also observed for polycarbonate by Senden *et al.* [92].

On the other hand, the temperature profile is responsible for two different effects,

480   depending on the time above and below the glass transition temperature T_g. Above T_g, molecular chain mobility is high enough to give the polymer the ability to (partially) relax its orientation and stretch. Below T_g, molecular mobility is much slower and relaxation can not occur. However, below the glass transition temperature, the thermodynamic state of the material changes due to physical aging [72, 19].

485   At a lower bed temperature, the difference between nozzle and bed temperatures is larger. Based on results reported by Sun *et al.* [23], this is expected to provoke higher temperature fluctuations, and the average and minimum temperatures to be lower. At higher printing velocities, the time between deposition of adjacent strands is lower,

19

resulting in an increase of the overall average temperature as well as the minimum
temperatures of the material, while lowering the time between peaks and the peak
values. This was demonstrated experimentally by Srinivas *et al.* [25] for PLA and
Abbott *et al.* [11] for ABS. At the higher bed temperature, average, minimum and
maximum temperatures rise [23]. As a consequence, the polymer may be more time,
or even constantly, above the glass transition temperature T_g, with possibly polymer
relaxation as a result. Furthermore, higher temperatures below T_g enhances physical
aging and a higher yield stress is the result [72, 19].

The highest yield stresses are encountered for the *v35o0T50* samples. Yet, porosity
is highest for this longitudinal sample set. If a lower porosity and higher elastic modu-
lus E is preferred, sets *v9o0T60* or *v35o0T60* would be the favored choice. These sets
also demonstrate a slightly higher ductility.

4.6. Transverse printing direction: $\alpha_{or} = 90°$

Figures 6(c) and 7(c) show the effect of printing velocity at a bed temperature
of $T_b = 50°C$. Again, velocity affects ductility and yield stress in a positive sense
for higher printing velocity. Besides, the strain rate at which the second deformation
process becomes visible, shifts to higher values for a higher printing velocity (see Fig-
ure 7(c)). Bustillos *et al.* [36] also observed an increase of the strain-rate dependence
at higher strain rates during indentation creep tests.

The above-described effect is inverted for the higher bed temperature $T_b = 60°C$
as can be seen in Figures 6(d) and 7(d): a lower velocity results in higher yield stresses.
Ductility is slightly lower for the low printing velocity, which may be attributed to the
higher yield stress. The strain rate at which the second molecular process starts to
interact is similar for both printing velocities.

For a printing velocity of $v_p = 35\ mm\ s^{-1}$, bed temperature effects can be seen
by comparing the open symbols in Figures 6(c) and 6(d) and the triangular symbols
in Figures 7(c) and 7(d). A lower bed temperature gives higher yield stresses and
improved ductility. Additionally, the change of slope shifts to a higher strain rate for
$T_b = 50°C$.

For a printing velocity of $v_p = 9\ mm\ s^{-1}$ (*i.e.* closed symbols in Figure 6(c)/6(d);
diamond and square symbols in Figure 7(c)/7(d)), again the inverse effect is seen: a
higher bed temperature gives higher stresses and ductility is slightly improved. The
effect on the change of slope is minimal, although at slightly higher strain rate for
$T_b = 60°C$.

As mentioned before, previous research by other groups have indicated that higher
velocities provoke the minimum temperatures to raise, the maximum temperatures to
decrease, and to reduce the time between peaks [25]. Furthermore, with a higher bed
temperature, the fluctuating temperature profile shifts completely to higher tempera-
tures [23]. The results for the transverse samples indicate that for lower bed tempera-
tures, higher printing speeds are preferred, as they provoke higher minimum tempera-
tures resulting in temperatures closer to T_g. That will result in higher yield stresses due
to physical aging.

On the contrary, lower printing speeds are beneficial for a higher bed temperature,
as those rise both the average as well as peak temperatures [23]. This seems to indicate

that the highest average temperature gives the best results for mechanical properties, provided that a certain minimum temperature is guaranteed.

535   The best mechanical properties are obtained for the *v35o90T50* set, both in yield stresses as well as ductility. Likewise, porosity is lowest for that set. The worst case scenario is given by results for the *v9o90T50* samples. Although yield stresses are similar to the *v35o90T60* sample set, this first mentioned set shows lower ductility and higher porosity.

540   *4.7. Influence of infill orientation*

There are differences in the yield drop for different sample sets. These can be best observed between samples at different orientations, as shown in Figure 8. There is also a small difference in yield drop at varying strain rates, see *e.g.* Figure 6(b). But that can be contributed to the so-called geometric softening.

545   At a printing velocity of $v_p = 35 \ mm \ s^{-1}$ (Figure 8(a)), the post-yield strain softening is significantly more pronounced for the longitudinal samples ($\alpha_{or} = 0°$; open symbols) than for the transverse samples ($\alpha_{or} = 90°$; closed symbols). It is still visible, although less apparent, in the plots for the low printing speed $v_p = 9 \ mm \ s^{-1}$ (Figure 8(b)). One can also detect a difference of the yield drop for different printing
550   speeds at an orientation of $90°$ by observing Figure 6(d). Hence, the yield drop seems to be related to the printing velocity, which implicates that it has a relation with the orientation and stretch of the molecular chains. That again, seems to indicate that strain hardening may be the cause of it all [92]. Yet, the fact that the tensile direction is parallel or perpendicular to the orientation direction is also of influence. The effect due
555   to different printing speeds is more pronounced in the transverse samples sets ($\alpha_{or} = 90°$), *i.e.* perpendicular to the orientation and stretch direction. The precise cause is yet unclear, and more research is necessary to clarify it.

(a)   (b)
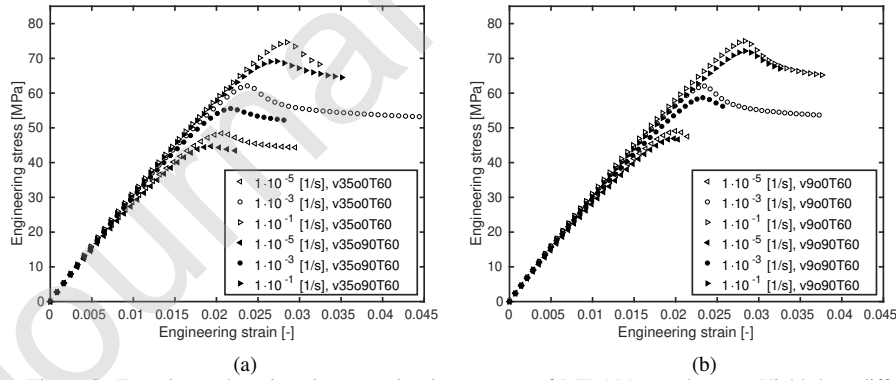
Figure 8: Experimental engineering stress/strain response of ME-AM samples. *(a)* Yield drop difference between $\alpha_{or} = 0°$ and $\alpha_{or} = 90°$ @$v_p = 35 \ mm \ s^{-1}$. *(b)* Yield drop difference between $\alpha_{or} = 0°$ and $\alpha_{or} = 90°$ @$v_p = 9 \ mm \ s^{-1}$.

In Figure 9, a comparison is made between the compression molded (*CM*) samples and two ME-AM sample sets without correcting for their porosity. One ME-AM

21

560 sample set is chosen that is printed with parameters giving among the highest yield stress values, both in the longitudinal direction ($\alpha_{or} = 0°$), as well as in the transverse direction ($\alpha_{or} = 90°$): *v35o0T50*. The other ME-AM sample set is chosen using processing parameters that give the lowest yield stress values in both directions, *i.e. v9o90T50*. Note that for comparison reasons, it is important to take into account the

565 strain rate at which the experimental data is obtained. For strain rates below $10^{-5} \; s^{-1}$, the *CM* results give the lowest values. For $10^{-5} \; s^{-1} < \dot{\varepsilon} < 10^{-3} \; s^{-1}$, the *CM* data are in between the two ME-AM sample sets. While for strain rates above approximately $2 \cdot 10^{-3} \; s^{-1}$, the *CM* sample set gives the highest values. Compare also the values given in Table 3.
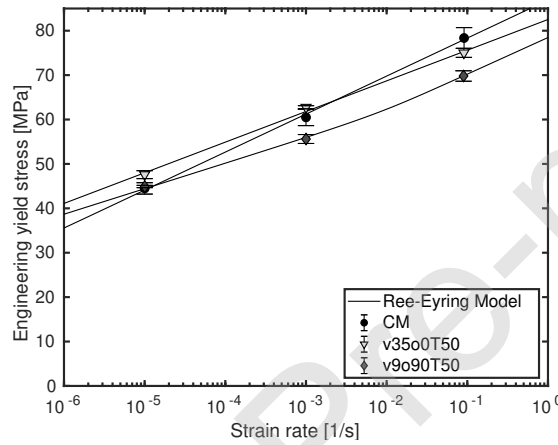
Figure 9: Engineering yield stress (without volume correction) as a function of logarithmic strain rate for *CM* (●), v35o0T50 (▽), and v9o90T50 (◆) samples. Symbols are experimental results, lines are model predictions.

570 As was mentioned before, the strain rate dependence of the yield stress is anisotropic for ME-AM samples and, moreover, is different from compression molded samples. This is very likely to also have its effect on long-term behavior, such as creep and fatigue, as was previously demonstrated [63, 64, 65, 66, 67]. In that sense, a lower strain rate dependence can be favorable for creep behavior at low stress values, improving its

575 time-to-failure [66]. This may be one of the advantages of ME-AM processing over conventional processes, such as compression or injection molding, and, if so, is yet to be exploited.

The results demonstrated in this section also show the importance of the temperature profile that material elements experience during processing on the resulting me-

580 chanical properties. That profile is completely dependent on the chosen printing parameters. As seen, the change of only one processing parameter (*i.e.* the bed temperature) can cause opposite effects on mechanical properties for other parameters.

22

5. Conclusions

The strain-rate dependence of the yield stress for ME-AM samples was measured
585 and analyzed. The apparent densities of the ME-AM processed tensile test specimens
were measured and taken into account in order to study the effects of the ME-AM
processing step on the material behavior. Three different printing parameters were
changed to investigate their influence on mechanical properties, *i.e.* infill velocity,
infill orientation angle, and bed temperature. Additionally, compression molded test
590 samples were manufactured in order to determine bulk properties, which have been
compared to the ME-AM sample sets.

As observed previously by other research groups, changing the infill orientation
angle from $0°$ to $90°$ displays anisotropic effects for ME-AM processed samples. Gen-
erally, the yield stresses measured in the longitudinal direction ($\alpha_{or} = 0°$) have higher
595 values compared to the transverse direction ($\alpha_{or} = 90°$). Although, by varying the
printing parameters, the opposite has also been measured in low strain-rate uniaxial
tensile tests (see Table 3).

Anisotropy has also been detected in the strain-rate dependence of the yield stresses.
Different slopes in the yield stress vs. logarithmic strain-rate plots are observed: ME-
600 AM samples with an infill angle of $0°$ have a higher strain-rate dependence than spec-
imens with $\alpha_{or} = 90°$. Besides, and this has not been reported to date, the slopes
manifested by the ME-AM samples is lower and significantly different from compres-
sion molded test specimens.

The Ree-Eyring modification of the Eyring flow rule is able to accurately describe
605 the strain-rate dependence of the yield stresses. In the case of the PLA material used in
the present research study, two molecular deformation processes are assumed to gov-
ern the yield kinetics. It was considered that (i) the yield kinetics of the CM samples
contain contributions of both processes ($\alpha + \beta$), (ii) yield stresses for low strain rates of
ME-AM samples printed at $\alpha_{or} = 90°$ are only controlled by the α-process, and (iii)
610 the enhanced slope observed for the longitudinal ($0°$) ME-AM samples is due to molec-
ular orientation. Subsequently, changes in yield stresses can then be accounted for by
changes in the activation volumes V^* and rate constants $\dot{\varepsilon}_0$. Although a wide strain-
rate range was applied, these assumptions are based on observation made on a relative
low number of strain rates. Hence, to improve the determination of the Ree-Eyring
615 model parameters and for a stronger experimental base of the above assumptions, mea-
surements for a higher number of strain rates will be beneficial.

All ME-AM sample sets show results relatively close to, but distinct from, the
results for the compression molding specimens. This manifests again that mechani-
cal properties can be achieved through ME-AM processing that are close to the bulk
620 properties. Notwithstanding, different results are obtained by varying printing param-
eters. Effects of changing ME-AM process parameters are not straightforward and,
occasionally, even opposite. Hence, it is complicated to understand the direct relation
between ME-AM processing parameters and the resulting mechanical properties. As
was shown by previous research [21, 23, 13, 22, 25] though, the temperature profile a
625 material element experiences over time is one of the most important aspects that deter-
mine mechanical properties. Likewise, strain and shear as a function of time also have
their effects [38, 35, 7], as is equally manifested by the results shown in this paper.

23

It is therefore more logically to research the relation between printing parameters and properties using an intermediate step, *i.e.* gaining knowledge about the temperature and strain profiles [37].

A remarkable effect encountered in our measurements is the fact that with some printing parameter sets, the results change from a brittle behavior in case of CM samples (and also seen in injection molded samples [10]) to a semi-ductile behavior for various ME-AM sets. This observation has been reported before [51, 10], and is attributed to the processing phase. Thus, the results reported here stress again the importance of the temperature profile (initial fast cooling combined with successive heating cycles) and the strain profile during ME-AM processing, which is significantly different from conventional processing methods (*e.g.* IM and CM). Such a transition may be beneficial for impact behavior [34], as the area under the stress-strain curve is increased.

The present study also manifests the importance of taking into account the strain rate at which the uniaxial tensile tests are performed. Results at low strain rate showed that yield stress values for CM samples were lower than ME-AM samples. On the other hand, the contrary was observed for high strain-rate tensile tests.

The experimental results shown here can be seen as initial work that can help to develop and improve quantitative predictive numerical tools for material extrusion additive manufacturing, as well as for the design of structural components, *e.g.* biomechanical utilities for elderly and disabled people. Not only is the strain-rate dependence important for short-term behavior, but it is known to also have its effect on long-term behavior [63, 64, 65, 66, 67]. In that sense, the lower strain-rate dependence as manifested for ME-AM samples made of PLA material compared to CM specimens may be exploited for structural components that, in service life, operate under static or dynamic loading conditions.

References

[1] S. Mellor, L. Hao, D. Zhang, Additive manufacturing: A framework for implementation, Int. J. Prod. Econ. 149 (2014) 194–201 (2014). doi:https://dx.doi.org/10.1016/j.ijpe.2013.07.008.

[2] ISO/ASTM 52900:2015, Additive manfucturing - General principles - Terminology (2015).

[3] B. Turner, R. Strong, S. Gold, A review of melt extrusion additive manufacturing processes: I. Process design and

24

modeling, Rapid Prototyp. J. 20 (3) (2014) 192–204 (2014). doi:http://dx.doi.org/10.1108/RPJ-01-2013-0012.

[4] J. Dizon, A. Espera Jr., Q. Chen, R. Advincula, Mechanical characterization of 3D-printed polymers, Addit. Manuf. 20 (2018) 44–67 (2018). doi:http://dx.doi.org/10.1016/j.addma.2017.12.002.

[5] T. Ngo, A. Kashani, G. Imbalzano, K. Nguyen, D. Hui, Additive manufacturing (3D printing): A review of materials, methods, applications and challenges, Composites B 143 (2018) 172–196 (2018). doi:http://dx.doi.org/10.1016/j.compositesb.2018.02.012.

[6] B. Wendel, D. Rietzel, F. Kühnlein, R. Feulner, G. Hülder, E. Schmachtenberg, Additive Processing of Polymers, Macromol. Mater. Eng. 293 (10) (2008) 799–809 (2008). doi:https://dx.doi.org/10.1002/mame.200800121.

[7] M. Mackay, The importance of rheological behavior in the additive manufacturing technique material extrusion, J. Rheol. 62 (6) (2018) 1549–1561 (2018). doi:https://dx.doi.org/10.1122/1.5037687.

[8] Z. Liu, Y. Wang, B. Wu, C. Cui, Y. Guo, C. Yan, A critical review of fused deposition modeling 3D printing technology in manufacturing polylactic acid parts, Int. J. Adv. Manuf. Techn. doi:10.1007/s00170-019-03332-x (2019). doi:http://dx.doi.org/10.1007/s00170-019-03332-x.

[9] M. Spoerk, F. Arbeiter, H. Cajner, J. Sapkota, C. Holzer, Parametric optimization of intra- and inter-layer strengths in parts produced by extrusion-based additive manufacturing of poly(lactid acid), J. Appl. Polym. Sci. 134 (41) (2017) 45401 (2017). doi:https://dx.doi.org/10.1002/app.45401.

[10] Y. Song, Y. Li, W. Song, K. Yee, K.-Y. Lee, V. Tagarielli, Measurements of the mechanical response of unidirectional 3D-printed PLA, Mater. Des. 123 (2017) 154–164 (2017). doi:https://dx.doi.org/10.1016/j.matdes.2017.03.051.

[11] A. Abbott, G. Tandon, R. Bradford, H. Koerner, J. Baur, Process-structure-property effects on ABS bond strength in fused filament fabrication, Addit. Manuf. 19 (2018) 29–38 (2018). doi:http://dx.doi.org/10.1016/j.addma.2017.11.002.

[12] J. Rodríguez, J. Thomas, J. Renaud, Mechanical behavior of acrylonitrile butadiene styrene (ABS) fused deposition materials. Experimental investigation, Rapid Prototyp. J. 7 (3) (2001) 148–158 (2001). doi:http://dx.doi.org/10.1108/13552540110395547.

[13] C. Kousiatza, D. Karalekas, In-situ monitoring of strain and temperature distributions during fused deposition modeling process, Mater. Des. 97 (2016) 400–406 (2016). doi:https://dx.doi.org/10.1016/j.matdes.2016.02.099.

[14] H. Niklas, H. Kausch von Schmeling, Molekularstruktur und mechanische Eigenschaften von Polyvinylchlorid III. Mitteilung: Ursachen zeitabhängiger Festigkeitseigenschaften von PVC-Rohren, Kunststoffe 53 (1963) 886–891 (1963).

[15] I. Narisawa, M. Ishikawa, H. Ogawa, Delayed yielding of polycarbonate under constant load, J. Polym. Sci. Polym. Phys. Ed. 16 (8) (1978) 1459–1470 (1978). doi:http://dx.doi.org/10.1002/pol.1978.180160811.

[16] H. van Melick, L. Govaert, H. Meijer, Localisation phenomena in glassy polymers: influence of thermal and mechanical history, Polymer 44 (12) (2003) 3579–3592 (2003). doi:http://dx.doi.org/10.1016/S0032-3861(03)00089-2.

[17] T. van Erp, L. Govaert, G. Peters, Mechanical Performance of Injection-Molded Poly(propylene): Characterization and Modeling, Macromol. Mater. Eng. 298 (3) (2013) 348–358 (2013). doi:http://dx.doi.org/10.1002/mame.201200116.

[18] D. Senden, G. Peters, L. Govaert, J. van Dommelen, Anisotropic yielding of injection molded polyethylene: Experiments and modeling, Polymer 54 (21) (2013) 5899–5908 (2013). doi:http://dx.doi.org/10.1016/j.polymer.2013.08.047.

[19] W. Verbeeten, M. Kanters, T. Engels, L. Govaert, Yield stress distribution in injection-moulded glassy polymers, Polym. Int. 64 (11) (2015) 1527–1536 (2015). doi:http://dx.doi.org/10.1002/pi.4898.

[20] J. Seppala, K. Migler, Infrared thermography of welding zones produced by polymer extrusion additive manufacturing, Addit. Manuf. 12 (2016) 71–76 (2016). doi:https://dx.doi.org/10.1016/j.addma.2016.06.007.

[21] J. Rodriguez, J. Thomas, J. Renaud, Characterization of the mesostructure of fused-deposition acrylonitrile-butadiene-styrene materials, Rapid Prototyp. J. 6 (3) (2000) 175–185 (2000). doi:http://dx.doi.org/10.1108/13552540010337056.

[22] J. Seppala, S. Han, K. Hillgartner, C. Davis, K. Migler, Weld formation during material extrusion additive manufacturing, Soft Matter 13 (2017) 6761–6769 (2017). doi:http://dx.doi.org/10.1039/c7sm00950j.

[23] Q. Sun, G. Rizvi, C. Bellehumeur, P. Gu, Effect of processing conditions on the bonding quality of FDM polymer filaments, Rapid Prototyp. J. 14 (2) (2008) 72–80 (2008). doi:http://dx.doi.org/10.1108/13552540810862028.

[24] F. Peng, B. Vogt, M. Cakmak, Complex flow and temperature history during melt extrusion in material extrusion additive manufacturing, Addit. Manuf. 22 (2018) 197–206 (2018). doi:https://dx.doi.org/10.1016/j.addma.2018.05.015.

26

[25] V. Srinivas, C. van Hooy-Corstjens, J. Harings, Correlating molecular and crystallization dynamics to macroscopic fusion and thermodynamic stability in fused deposition modeling; a model study on polylactides, Polymer 142 (2018) 348–355 (2018). doi:http://dx.doi.org/10.1016/j.polymer.2018.03.063.

[26] C. McIlroy, P. Olmsted, Disentanglement effects on welding behaviour of polymer melts during the fused-filament-fabrication method for additive manufacturing, Polymer 123 (2017) 376–391 (2017). doi:http://dx.doi.org/10.1016/j.polymer.2017.06.051.

[27] W. Schneider, A. Köpple, J. Berger, Non-isothermal crystallization of polymers, Int. Polym. Process. 2 (3-4) (1988) 151–154 (1988). doi:http://dx.doi.org/10.3139/217.880150.

[28] H. Zuidema, G. Peters, H. Meijer, Influence of cooling rate on PVT-data of semi-crystalline polymers, J. Appl. Polym. Sci. 82 (5) (2001) 1170–1186 (2001). doi:http://dx.doi.org/10.1002/app.1951.

[29] I. Coccorullo, R. Pantani, G. Titomanlio, Crystallization kinetics and solidified structure in iPP under high cooling rates, Polymer 44 (1) (2003) 307–318 (2003). doi:http://dx.doi.org/10.1016/S0032-3861(02)00762-0.

[30] R. Zheng, P. Kennedy, A model for post-flow induced crystallization: General equations and predictions, J. Rheol. 48 (4) (2004) 823–842 (2004). doi:http://dx.doi.org/10.1122/1.1763944.

[31] R. Popli, L. Mandelkern, Influence of structural and morphological factors on the mechanical properties of the polyethylenes, J. Polym. Sci. Part B: Polym. Phys. 25 (3) (1987) 441–483 (1987). doi:http://dx.doi.org/10.1002/polb.1987.090250301.

[32] D. Grijpma, A. Pennings, (Co)polymers of L-lactide, 2. Mechanical properties, Macromol. Chem. Phys. 195 (5) (1994) 1649–1663 (1994). doi:http://dx.doi.org/10.1002/macp.1994.021950516.

[33] B. Schrauwen, R. Janssen, L. Govaert, H. Meijer, Intrinsic deformation behavior of semicrystalline polymers, Macromolecules 37 (16) (2004) 6069–6078 (2004). doi:http://dx.doi.org/10.1021/ma035279t.

[34] L. Wang, W. Gramlich, D. Gardner, Improving the impact strength of Poly(lactid acid) (PLA) in fused layer modeling (FLM), Polymer 114 (2017) 242–248 (2017). doi:http://dx.doi.org/10.1016/j.polymer.2017.03.011.

[35] C. McIlroy, R. Graham, Modelling flow-enhanced crystallisation during fused filament fabrication of semi-crystalline polymer melts, Addit. Manuf. 24 (2018) 323–340 (2018). doi:https://dx.doi.org/10.1016/j.addma.2018.10.018.

27

[36] J. Bustillos, D. Montero, P. Nautiyal, A. Loganathan, B. Boesl, A. Agarwal, Integration of Graphene in Poly(Lactic) Acid by 3D Printing to Develop Creep and Wear-Resistant Hierarchical Nanocomposites, Polym. Compos. 39 (11) (2018) 3877–3888 (2018). `doi:http://dx.doi.org/10.1002/pc.24422`.

[37] L. Northcutt, S. Orski, K. Migler, A. Kotula, Effect of processing conditions on crystallization kinetics during materials extrusion additive manufacturing, Polymer 154 (2018) 182–187 (2018). `doi:http://dx.doi.org/10.1016/j.polymer.2018.09.018`.

[38] C. McIlroy, P. Olmsted, Deformation of an amorphous polymer during the fused-filament-fabrication method for additive manufacturing, J. Rheol. 61 (2) (2017) 379–397 (2017). `doi:http://dx.doi.org/10.1122/1.4976839`.

[39] T. Coogan, D. Kazmer, In-line rheological monitoring of fused deposition modeling, J. Rheol. 63 (1) (2019) 141–155 (2019). `doi:https://dx.doi.org/10.1122/1.5054648`.

[40] H. Giesekus, A simple constitutive quation for polymer fluids based on the concepts of deformation-dependent tensorial mobility, J. Non-Newtonian Fluid Mech. 11 (1-2) (1982) 69–109 (1982). `doi:http://dx.doi.org/10.1016/0377-0257(82)85016-7`.

[41] N. Phan-Thien, R. I. Tanner, A new constitutive equation derived from network theory, J. Non-Newtonian Fluid Mech. 2 (4) (1977) 353–365 (1977). `doi:http://dx.doi.org/10.1016/0377-0257(77)80021-9`.

[42] R. I. Tanner, Engineering Rheology, 2nd Edition, Oxford University Press, London, 2000 (2000).

[43] W. Verbeeten, G. Peters, F. Baaijens, Differential constitutive equations for polymer melts: The extended Pom-Pom model, J. Rheol. 45 (4) (2001) 823–843 (2001). `doi:http:/dx.doi.org/10.1122/1.1380426`.

[44] W. Verbeeten, G. Peters, F. Baaijens, Numerical simulations of the planar contraction flow for a polyethylene melt using the XPP model, J. Non-Newtonian Fluid Mech. 117 (2-3) (2004) 73–84 (2004). `doi:http://dx.doi.org/10.1016/j.jnnfm.2003.12.003`.

[45] E. Narimissa, M. Wagner, Review on tube model based constitutive equations for polydisperse linear and long-chain branched polymer melts, J. Rheol. 63 (2) (2019) 361–375 (2019). `doi:http://dx.doi.org/10.1122/1.5064642`.

[46] A. Likhtman, R. Graham, Simple constitutive equation for linear polymer melts derived from molecular theory: Rolie-Poly equation, J. Non-Newtonian Fluid Mech. 114 (1) (2003) 1–12 (2003). `doi:http://dx.doi.org/10.1016/S0377-0257(03)00114-9`.

28

[47] K. Hart, R. Dunn, J. Sietins, C. Hofmeister Mock, M. Mackay, E. Wetzel, Increased fracture toughness ad additively manufactured amorphous thermoplastics via thermal annealing, Polymer 144 (2018) 192–204 (2018). doi:http://dx.doi.org/10.1016/j.polymer.2018.04.024.

[48] F. Yang, R. Pitchumani, Interlaminar contact development during thermoplastic fusion bonding, Polym. Eng. Sci. 42 (2) (2002) 424–438 (2002). doi:http://dx.doi.org/10.1002/pen.10960.

[49] B. Tymrak, M. Kreiger, J. Pearce, Mechanical properties of components fabricated with open-source 3-D printers under realistic environmental conditions, Mater. Des. 58 (2014) 242–246 (2014). doi:http://dx.doi.org/10.1016/j.matdes.2014.02.038.

[50] M. Afrose, S. Masood, P. Iovenitti, M. Nikzad, I. Sbarski, Effects of part build orientations on fatigue behaviour of FDM-processed PLA material, Prog. Addit. Manuf. 1 (1-2) (2016) 21–28 (2016). doi:http://dx.doi.org/10.1007/s40964-015-0002-3.

[51] J. Chacón, M. Caminero, E. García-Plaza, P. Núñez, Additive manufacturing of PLA structures using fused deposition modelling: Effect of process parameters on mechanical properties and their optimal selection, Mater. Des. 124 (2017) 143–157 (2017). doi:http://dx.doi.org/10.1016/j.matdes.2017.03.065.

[52] B. Wittbrodt, J. Pearce, The effects of PLA color on material properties of 3-D printed components, Addit. Manuf. 8 (2015) 110–116 (2015). doi:https://dx.doi.org/10.1016/j.addma.2015.09.006.

[53] A. Lanzotti, M. Grasso, G. Staiano, M. Martorelli, The impact of process parameters on mechanical properties of parts fabricated in PLA with an open-source 3-D printer, Rapid Prototyp. J. 21 (5) (2015) 604–617 (2015). doi:http://dx.doi.org/10.1108/RPJ-09-2014-0135.

[54] F. Arbeiter, M. Spoerk, J. Wiener, A. Gosch, G. Pinter, Fracture mechanical characterization and lifetime estimation of near-homogeneous components produced by fused filament fabrication, Polym. Test. 66 (2018) 105–113 (2018). doi:https://dx.doi.org/10.1016/j.polymertesting.2018.01.002.

[55] T. Tervoort, E. Klompen, L. Govaert, A multi-mode approach to finite, three-dimensional, nonlinear viscoelastic behavior of polymer glasses, J. Rheol. 40 (5) (1996) 779–797 (1996). doi:http://dx.doi.org/10.1122/1.550755.

[56] L. van Breemen, E. Klompen, L. Govaert, H. Meijer, Extending the EGP constitutive model for polymer glasses to multiple relaxation times, J. Mech. Phys. Solids 59 (10) (2011) 2191–2207 (2011). doi:http://dx.doi.org/10.1016/j.jmps.2011.05.001.

[57] H. Eyring, Viscosity, Plasticity, and Diffusion as Examples of Abso-
865   lute Reaction Rates, J. Chem. Phys. 4 (4) (1936) 283–291 (1936).
doi:http://dx.doi.org/10.1063/1.1749836.

[58] T. Ree, H. Eyring, Theory of Non-Newtonian Flow. I. Solid
Plastic System, J. Appl. Phys. 26 (7) (1955) 793–800 (1955).
doi:http://dx.doi.org/10.1063/1.1722098.

870 [59] R. Haward, G. Thackray, The Use of a Mathematical Model to Describe Isother-
mal Stress-Strain Curves in Glassy Thermoplastics, Proc. Royal Soc. Lon-
don, Series A: Math., Phys. Eng. Sci. 302 (1471) (1968) 453–472 (1968).
doi:http://dx.doi.org/10.1098/rspa.1968.0029.

[60] C. Bauwens-Crowet, J. Bauwens, G. Homès, Tensile yieldstress behavior of
875   glassy polymers, J. Polym. Sci. Part A-2: Polym. Phys. 7 (4) (1969) 735–742
(1969). doi:http://dx.doi.org/10.1002/pol.1969.160070411.

[61] E. Klompen, L. Govaert, Nonlinear Viscoelastic Behaviour of Thermorheologi-
cally Complex Materials, Mech. Time-Dep. Mater. 3 (1) (1999) 49–69 (1999).
doi:http://dx.doi.org/10.1023/A:1009853024441.

880 [62] L. van Breemen, T. Engels, E. Klompen, D. Senden, L. Govaert,
Rate- and Temperature-Dependent Strain Softening in Solid Polymers, J.
Polym. Sci. Part B: Polym. Phys. 50 (24) (2012) 1757–1771 (2012).
doi:http://dx.doi.org/10.1002/polb.23199.

[63] E. Klompen, T. Engels, L. van Breemen, P. Schreurs, L. Gov-
885   aert, H. Meijer, Quantitative Prediction of Long-Term Failure of
Polycarbonate, Macromolecules 38 (16) (2005) 7009–7017 (2005).
doi:http://dx.doi.org/10.1021/ma0504973.

[64] R. Janssen, D. de Kanter, L. Govaert, H. Meijer, Fatigue Life Predictions for
Glassy Polymers: A Constitutive Approach, Macromolecules 41 (7) (2008)
890   2520–2530 (2008). doi:http://dx.doi.org/10.1021/ma071273i.

[65] H. Visser, T. Bor, M. Wolters, T. Engels, L. Govaert, Lifetime Assess-
ment of Load-Bearing Polymer Glasses: An Analytical Framework for
Ductile Failure, Macromol. Mater. Eng. 295 (7) (2010) 637–651 (2010).
doi:http://dx.doi.org/10.1002/mame.200900369.

895 [66] T. Engels, S. Söntjens, T. Smit, L. Govaert, Time-dependent
failure of amorphous polylactides in static loading condi-
tions, J. Mater. Sci.-Mater. Med. 21 (1) (2010) 89–97 (2010).
doi:http://dx.doi.org/10.1007/s10856-009-3851-9.

[67] M. Kanters, K. Remerie, L. Govaert, A new protocol for acceler-
900   ated screening of longterm plasticitycontrolled failure of polyethy-
lene pipe grades, Polym. Eng. Sci. 56 (6) (2016) 676–688 (2016).
doi:https://dx.doi.org/10.1002/pen.24294.

[68] A. Vairis, M. Petousis, N. Vidakis, K. Savvakis, On the Strain Rate Sensitivity of Abs and Abs Plus Fused Deposition Model-ing Parts, J. Mater. Eng. Perf. 25 (9) (2016) 3558–3565 (2016). doi:http://dx.doi.org/10.1007/s11665-016-2198-x.

[69] M. Boyce, D. Parks, A. Argon, Large inelastic deformation of glassy polymers. part I: rate dependent constitutive model, Mech. Mater. 7 (1) (1988) 15–33 (1988). doi:http://dx.doi.org/10.1016/0167-6636(88)90003-8.

[70] P. Wu, E. van der Giessen, On improved network models for rub-ber elasticity and their applications to orientation hardening in glassy polymers, J. Mech. Phys. Solids 41 (3) (1993) 427–456 (1993). doi:http://dx.doi.org/10.1016/0022-5096(93)90043-F.

[71] C. Buckley, D. Jones, Glass-rubber constitutive model for amorphous poly-mers near the glass transition, Polymer 36 (17) (1995) 3301–3312 (1995). doi:http://dx.doi.org/10.1016/0032-3861(95)99429-X.

[72] E. Klompen, T. Engels, L. Govaert, H. Meijer, Modeling of the Postyield Response of Glassy Polymers: Influence of Thermome-chanical History, Macromolecules 38 (16) (2005) 6997–7008 (2005). doi:http://dx.doi.org/10.1021/ma050498v.

[73] B. Schrauwen, L. van Breemen, A. Spoelstra, L. Govaert, G. Peters, H. Meijer, Structure, deformation, and failure of flow-oriented semi-crystalline polymers, Macromolecules 37 (23) (2004) 8618–8633 (2004). doi:http://dx.doi.org/10.1021/ma048884k.

[74] J. Roetling, Yield Stress Behaviour of Polymethyl-methacrylate, Polymer 6 (6) (1965) 311–317 (1965). doi:http://dx.doi.org/10.1016/0032-3861(65)90081-9.

[75] C. Bauwens-Crowet, The compression yield behaviour of polymethyl methacry-late over a wide range of temperatures and strain-rates, J. Mater. Sci. 8 (7) (1973) 968–979 (1973). doi:https://dx.doi.org/10.1007/BF00756628.

[76] E. Fischer, H. Sterzel, G. Wegner, Investigation of the structure of so-lution grown crystals of lactide copolymers by means of chemical reac-tions, in: E. Fischer, F. Müller, H. Kausch (Eds.), Aktuelle Probleme der Polymer-Physik IV, Vol. 4, Steinhopff, 1973, pp. 980–990 (1973). doi:https://dx.doi.org/10.1007/978-3-642-47050-9_24.

[77] C. Bauwens-Crowet, J.-C. Bauwens, G. Homès, The Tempera-ture Dependence of Yield of Polycarbonate in Uniaxial Compres-sion and Tensile Tests, J. Mater. Sci. 7 (2) (1972) 176–183 (1972). doi:http://dx.doi.org/10.1007/BF00554178.

[78] I. Ward, Review: The Yield Behaviour of Polymers, J. Mater. Sci. 6 (11) (1971) 1397–1417 (1971). doi:http://dx.doi.org/10.1007/BF00549685.

[79] L. Govaert, P. Timmermans, W. Brekelmans, The Influence of Intrinsic Strain Solftening on Strain Localization in Polycarbonate: Modeling and Experimental Validation, J. Eng. Mater. Technol. 122 (2) (2000) 177–185 (2000). doi:http://dx.doi.org/10.1115/1.482784.

[80] J. Sauer, D. Mears, K. Pae, Effects of hydrostatic pressure on the mechanical behaviour of polytetrafluoroethylene and polycarbonate, Eur. Polym. J. 6 (7) (1970) 1015–1022 (1970). doi:https://dx.doi.org/10.1016/0014-3057(70)90034-0.

[81] S. Rabinowitz, I. Ward, J. Parry, The effect of hydrostatic pressure on the shear yield behaviour of polymers, J. Mater. Sci. 5 (1) (1970) 29–39 (1970). doi:http://dx.doi.org/10.1007/BF02427181.

[82] A. Christiansen, E. Baer, S. Radcliffe, The Mechanical Behaviour of Polymers under High Pressure, Philos. Mag. 24 (188) (1971) 451–467 (1971). doi:http://dx.doi.org/10.1080/14786437108227400.

[83] K. Pae, S. Bhateja, The Effects of Hydrostatic Pressure on the Mechanical Behavior of Polymers, J. Macromol. Sci. C 13 (1) (1975) 1–75 (1975). doi:http://dx.doi.org/10.1080/15321797508068145.

[84] F. Carrasco, P. Pagès, J. Gámez-Pérez, O. Santana, M. Maspoch, Processing of poly(lactic acid): Characterization of chemical structure, thermal stability and mechanical properties, Polym. Degrad. Stab. 95 (2) (2010) 116–125 (2010). doi:https://dx.doi.org/10.1016/j.polymdegradstab.2009.11.045.

[85] L. Govaert, H. Schellens, H. Thomassen, R. Smit, L. Terzoli, T. Peijs, A micromechanical approach to time-dependent failure in off-axis loaded polymer composites, Composites A 32 (12) (2001) 1697–1711 (2001). doi:http://dx.doi.org/10.1016/S1359-835X(01)00028-8.

[86] J. Andrews, I. Ward, The cold-drawing of high density polyethylene, J. Mater. Sci. 5 (5) (1972) 411–417 (1972). doi:http://dx.doi.org/10.1007/BF00550003.

[87] T. Liu, I. Harrison, Effect of draw rate on the stress-strain behaviour of polymers, Polymer 29 (2) (1988) 233–239 (1988). doi:http://dx.doi.org/10.1016/0032-3861(88)90327-8.

[88] R. Haward, The application of a Gauss-Eyring model to predict the behavior of thermoplastics in tensile experiments, J. Polym. Sci. Part B: Polym. Phys. 33 (10) (1995) 1481–1494 (1995). doi:http://dx.doi.org/10.1002/polb.1995.090331005.

[89] R. Truss, P. Clarke, R. Duckett, I. Ward, The dependence of yield behavior on temperature, pressure, and strain rate for linear polyethylenes of different molecular weight and morphology, J. Polym. Sci. Polym. Phys. Ed. 22 (2) (1984) 191–209 (1984). doi:http://dx.doi.org/10.1002/pol.1984.180220205.

[90] H. Urayama, T. Kanamori, Y. Kimura, Microstructure and Thermome-chanical Properties of Glassy Polylactides with Different Optical Purity of the Lactate Units, Macromol. Mater. Eng. 286 (11) (2001) 705–713 (2001). doi:https://dx.doi.org/10.1002/1439-2054(20011101)286:11<705::AID-MAME705>3.

[91] T. van Erp, C. Reynolds, T. Peijs, J. van Dommelen, L. Govaert, Predic-tion of yield and long-term failure of oriented polypropylene: Kinetics and anisotropy, J. Polym. Sci. Part B: Polym. Phys. 47 (20) (2009) 2026–2035 (2009). doi:http://dx.doi.org/10.1002/polb.21801.

[92] D. Senden, J. van Dommelen, L. Govaert, Strain hardening and its relation to Bauschinger effects in oriented polymers, J. Polym. Sci. Part B: Polym. Phys. 48 (13) (2010) 1483–1494 (2010). doi:http://dx.doi.org/10.1002/polb.22056.

33

May 28, 2019

Highlights for the article *Anisotropic rate-dependent mechanical behavior of Poly(Lactic Acid) processed by Material Extrusion Additive Manufacturing*:

- Strain-rate dependence is anisotropic in Material Extrusion Additive Manufacturing.

- Strain-rate dependence in ME-AM is different from compression molded products.

- Ree-Eyring flow rule can adequately describe the yield kinetics of ME-AM components.

- Compression molded samples show brittle stress-strain behavior.

- Several ME-AM samples show semi-ductile stress-strain behavior.

Graphical Abstract: